Volume 17, Issue 4, 172528 (1-11)

Iranian Journal of Earth Science (IJES)

https://doi.org/10.57647/j.ijes.2025.16949

Using the three dimensional statistical and multifractal models to determine of Pb-Zn anomalies in the Khomain area, Sanandaj Sirjan belt, western Iran

Feridon Ghadimi[1,*], Massume Khavari[1], Hossein Azizi[2]

[1]*Department of Mining Engineering, Arak University of Technology, Arak, Iran.*
[2]*Department of Mining, Faculty of Engineering Unversity of Kurdistan, Sanandaj, Iran.*

[*]**Corresponding author:** ghadimi@arakut.ac.ir

Original Research

Received:
2024-12-29
Revised:
2025-02-16
Accepted:
2025-02-28
Published online:
2025-06-24
Published in issue:
2025-10-30

Abstract:

Khomain deposit is situated in the western north part of the Sanandaj-Sirjan belt in western Iran. The main host rocks of the mineralization zone are shale, sandstone Jurassic to lower Cretaceous limestone. Main mineralization deposit includes galena and sphalerite minerals in Khomain. In this research, 170 samples from 33 boreholes were selected to determine the possibility of Pb and Zn anomalies. Lower geochemical anomalies determined by statistical and multifractal models. The Lepeltier, composite halo, factor analysis, original singularity and weighted singularity models were used to identify three dimension anomaly. The coefficient of areal association (CAA) is used to determine similarity of results of different models and is 0.90 and 0.61 for Pb and Zn in weighted singularity model. It indicated that Pb and Zn were confirmed by weighted singularity model in three dimensional studies. Therefore, it can be said that weighted singularity model is suitable relative to other models in identifying weak anomalies. It was determined that the mineralization has a northeast-southwest trend based on the weighted singularity models and is matches with the trend of faults in the mineralization place.

Keywords: Pb-Zn deposits; Singularity models; Khomain; Sandaj-Sirjan zone; Jurassic mineralization

1. Introduction

The separation of geochemical anomalies reflects geochemical processes and is one of the aims of exploration (Karami and Afzal, 2015; Wang and Zuo, 2019; Hu et al., 2023). Anomalous patterns caused by mineralization processes are very complex in the Pb-Zn deposits in terms of location and abundance (Huang et al., 2019a; Liu et al., 2019; Vincent et al., 2021; Zhu et al., 2022b). Accurate separation of spatial features is very important in identifying weak anomalies (Cheng, 2007). The separation of weak anomalies is a very difficult due to the influence of different geological units (Zhao et al., 2015). In other words, it is not possible to separate weak anomalies by analyzing primary data alone in the Pb-Zn deposits (Yu et al., 2020; Zhang et al., 2020; Zhu et al., 2022a). Determination of weak anomalies is one of the most important challenges in exploration geochemistry (Cheng et al., 2011; Huang et al., 2019b).
The median-standard deviation model is a common model to determine the threshold. Threshold is determined by (Median)+2S in exploration geochemistry. In other words, values larger than (Median)+2S will be considered as anomalies (Reimann et al., 2005). This model can only detect the threshold values/mean of background values will give us weak or strong anomaly. Several multivariate data analysis (e.g., factor analysis, cluster analysis, etc.) and fractal/multifractal models have been developed and effectively applied in exploration geochemical data for defining and mapping anomalies. Singularity model is one of the most important models for separating the weak anomalies (Parsa et al., 2017b; Afzal et al., 2017; Sadeghi, 2021; Fan et al., 2024; Elmi et al., 2025). Singularity model evaluates relative slope of changes in small distances (Luo and Zeng, 2018; Bigdeli et al., 2023) and is a strong way to recognizing weak anomalies (Arjmandzadeh et al., 2017; Gonçalves et al., 2018; Nazari Sarem et al., 2020; Liu and Carranza, 2022; Saadat et al., 2023). Several researchers

have improved to demonstrate geochemical anomalies by combination of singularity model along with other methods (Parsa et al., 2017a; Zhao et al., 2017; Chen et al., 2018; Xiao et al., 2018; Yazdi et al., 2019; Behera and Naliy Panigrah, 2021; Zhou et al., 2022). Singularity model has been developed in original singularity and weighted singularity model for detecting anisotropic patterns (Ghadimi and Khavari, 2019; Salehpour et al., 2025). The mineralization associated with geochemical anomalies in mineral exploration and usually are characterized by anisotropic patterns. Anisotropic patterns are controlled by the ore-controlling geological features (such as strata, faults, folds, and magma intrusions) (Zhang et al., 2016). Weighted singularity index is a useful tool for detecting features with anisotropic patterns and is without relation to samples or variables in the geo information extraction (Zhao et al., 2016).

The purpose of this research is to determine geochemical anomalies by different tree dimension statistical and singularity models and select the best model to define anomaly of the Pb-Zn concentration in the subsurface part of the Khomain area.

2. Geology of the region

Khomain deposit is located in southwest of Khomein in Sanandaj-Sirjan belt (Fig. 1). There are about 220 deposits in the Sanandaj-Sirjan belt (Taylor et al., 2009; Alipoor et al., 2021). All these deposits have occurred in the lower Cretaceous carbonate facies (about 90%) and Jurassic sandstone and shale (about 10%). Jurassic in the region includes shale, sandstone, and Cretaceous includes limestone and dolomitic limestone (Fig. 2). The texture is in the form of stratification in mineralization. Mineralization includes galena, pyrite, sphalerite, chalcopyrite, iron oxides, iron carbonate. The mineralization is SEDEX type by the ratios of Pb+Zn, Pb/Pb+Zn and Cu+Pb+Zn and Cu compounds. Shales and sandstones have been affected by silica, dolomite and sericite hydrothermal alteration with the movement of mineralizing solutions along normal faults (Zandy Ilghani et al., 2018).

3. Materials and methods

3.1 Sampling and analysis

One hundred seventy samples were selected from 33 boreholes with an average depth of 50 meters and intervals of 100 meters from Khomain area (Fig. 3). Samples were selected from three vertical sections (63 samples in the first, 48 samples from the second, and 59 samples in the third sections (Zandy Ilghani et al., 2018) (Fig. 3). Samples crushed and pulverized up to 200 mesh diameter. About 20 grams of the samples are taken after initial homogenization for the analysis of ICP method. Samples were analyzed for Pb, Zn with the ICP-MS device by the method of four acids (HF,

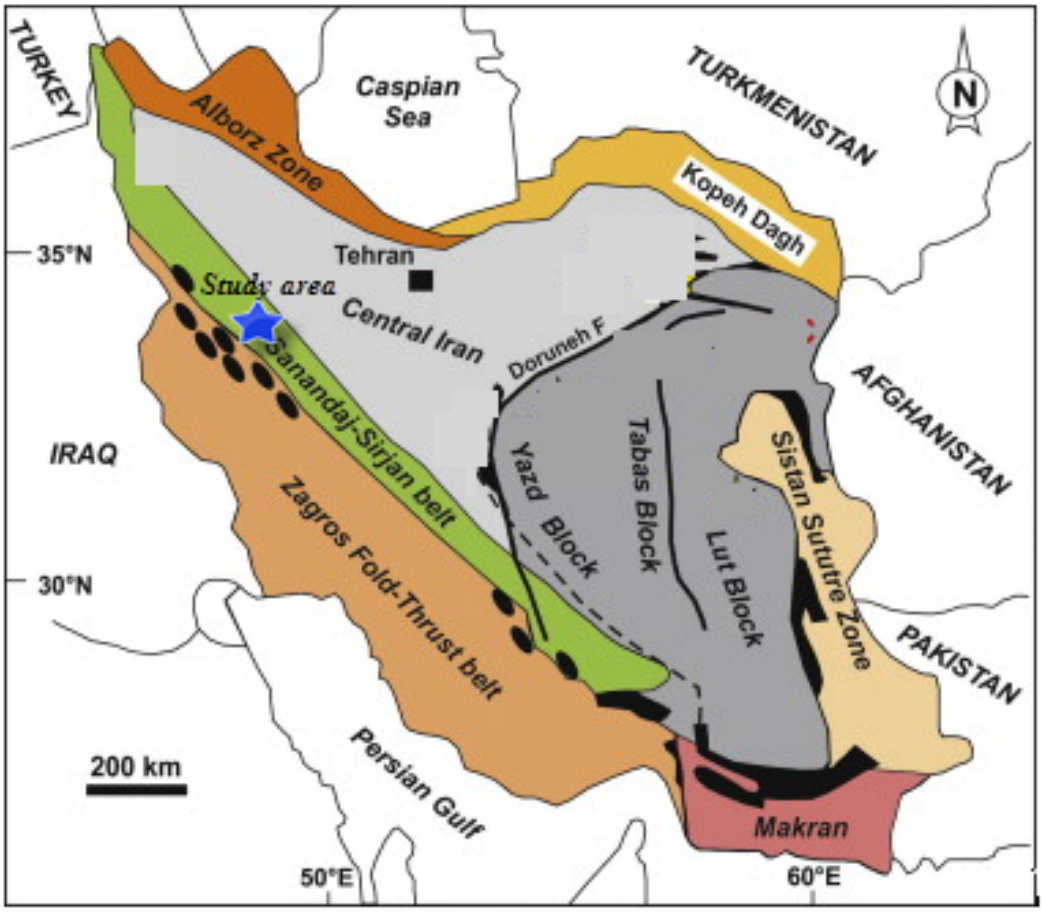

Figure 1. Khomain Pb-Zn deposit in Sanandaj-Sirjan geological belt (Stocklin and Nabavi, 1972).

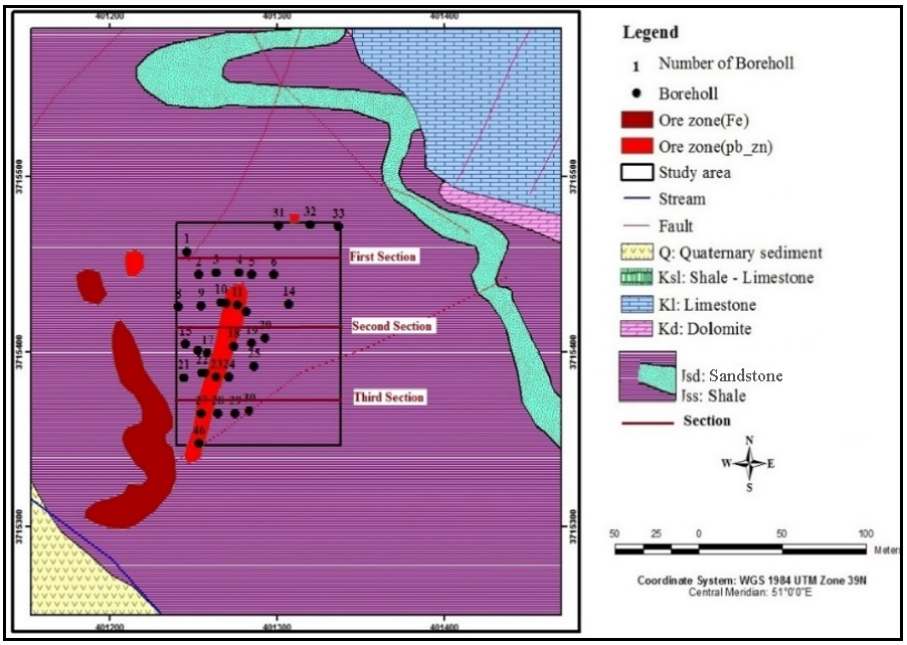

Figure 2. Summary of geological units of Khomain area (Ghadimi and Khavari, 2019).

HCl, $HClO_4$ and HNO_3). The accuracy limit was 1 mg/kg for Pb and Zn and the accuracy of calculations is less than 10%.

3.2 Methods

Appropriate transformations has be done on the data in order to use standard statistical data. Central log ratio method is selected for transformation data Eq. (1).

$$clr(x) = \ln \frac{x_i}{x_j} \tag{1}$$

where, x is the initial value and x_j is the geometric mean of the data.

Lepeltier model (median-standard deviation) is a common model for estimating threshold and shows some disadvantages compared to other models (Reimann et al., 2005). This model can only detect strong anomalies in a background and does not have the power to detect weak anomalies. Factor analysis were selected for identifying mineralization zones by geochemical indices. Composite halo is dimensionless quantities. Mineralization composite halo are the most reliable criteria in determining the initial aureoles on the deposit, the erosion level of the deposit, and evaluating the mineralization in depth (Zandy Ilghani et al., 2018). Composite halo have a uniform behavior in the overall depth

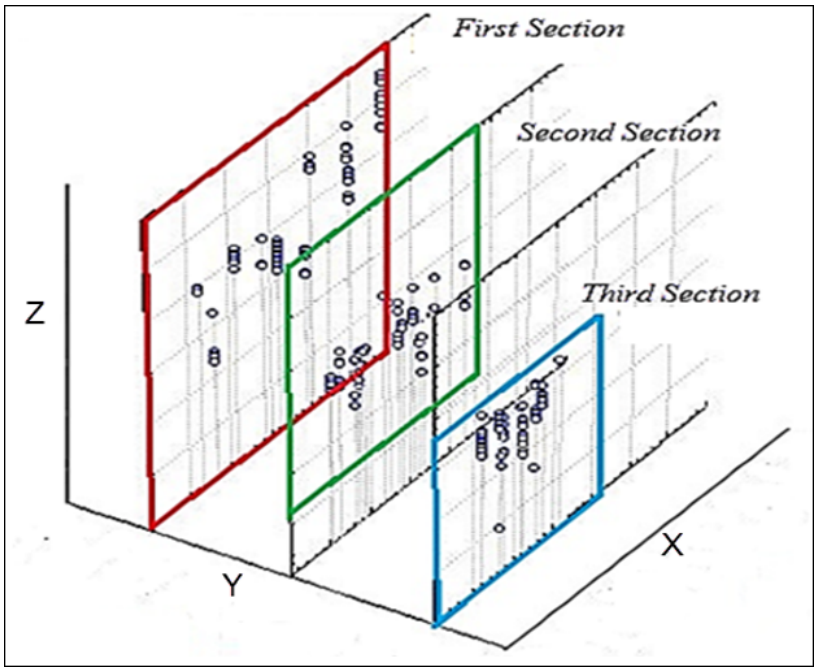

Figure 3. Sampling location in the 3D diagram of Khomain area (Ghadimi and Khavari, 2019).

of the deposit (they increase or decrease uniformly with depth). Participating metals in composite halo should be different from each other as much as possible. Zn/Pb and Zn/Pb+Zn indices were used in this manuscript.

Factor analysis used in order to determine the relationship between variables. Factor analysis is a specific relationship under a hypothetical model between a set of different variables. Therefore, one of the main aims of the factor analysis technique is to reduce the dimensions of the data. The basic assumption in using this technique is the existence of an infrastructure model or a linear model in determining the complex concepts of communication between variables. This relationship appears as a factor in this hypothetical model.

Fuzzification can solve the range of variable scores in the factors Eq. (2). Variable scores was converted in the range of zero to one according to Eq. (2) (Yousefi et al., 2012). Three-dimensional factorial fuzzy map was drawn in RockWorks software.

$$\mathrm{GMPI} = \frac{e^{FS}}{1+e^{FS}} \tag{2}$$

where GMPI is the probability index of geochemical mineralization and FS is the factorial score for each sample.

Singularity is defined based on the Law-power model (Cheng, 2008). The amount of the metal in the volume of the deposit (V) is $\mu(V)$. Therefore, the concentration $C(V)$ of the metal according to the volume V is expressed as Eq. (3).

$$C(V) = \mu(V)/V \tag{3}$$

The values of $C(V)$ and $\mu(V)$ follow a power-law equation (Eq. (4), (5)) according to the multifractal model.

$$M(V) = cV^{\frac{\alpha}{3}} \tag{4}$$

$$C(V) = cV^{\frac{\alpha}{3}-1} \tag{5}$$

where $\mu(V)$ is the amount of metal in V and $C(V)$ is the average concentration of V, c is a constant value and α is the power-law interface. Eq. (4), (5) show this relationship in three dimensions. The power α is called singularity index in multifractal models (Cheng, 2008). The value of power α is classified into two groups: $C(V)$ has no relationship with V and $\alpha = 3$. $C(V)$ is dependent on V, so $\alpha \neq 3$. The first group is non-singular and the second group is singular. The positivity of the singularity index shows the enrichment and the negativity shows the depletion index of the mineral (Ali et al., 2015). The main singularity index is estimated according to the smallest neighborhood based on Eq. (6).

$$C = c \cdot \varepsilon^{(\alpha - E)} \tag{6}$$

Here, C is the average metal concentration, c a constant value, α singularity index, ε normalized distance, and E is the euclidean geometry (Cheng, 2007). The desired value has a linear trend on the logarithmic graph (Eq. (7)).

$$\log C[V(r)] = c + (\alpha - 3)\log(r) \tag{7}$$

The slope of the estimate is $\alpha - 3$ in the linear relationship (Eq. (7)). The calculation windows are wide in the original singularity model, therefore, the weighted singularity index is usually used. The weights are determined according to the distance of a point to the unknown point. The closest point has more weight (Eq. (8)).

$$C = \frac{\frac{c_1}{d_1^n} + \frac{c_2}{d_2^n} + \cdots + \frac{c_m}{d_m^n}}{\frac{1}{d_1^n} + \frac{1}{d_2^n} + \cdots + \frac{1}{d_m^n}} \tag{8}$$

We must introduce the minimum concentration as the background and subtract it from the total data values in order to calculate the weak normality.

4. Results and discussion

4.1 Descriptive statistics

Descriptive statistics for Pb and Zn are shown in Table 1. The mean Pb and Zn concentration is equal to 5381 and 7268 mg/kg, respectively.

4.2 Lepeltier model

It used Lepeltier model for detecting the metals anomaly. The values of (Median)+2S (S is standard deviation) was calculated for each metals (Reimann et al., 2005). 3D models of fuzzy Pb and Zn concentrations were created based on the kriging method (**Panahi etal 2004?**). Fuzzy Pb and Zn is highly enriched in the region. High Pb and Zn values have a wide distribution in the southwest part of the region (Fig. 4 a, b). Lepelier index showed that Pb background limit is 4000 mg/kg, the threshold 7000 mg/kg and anomaly limit is 10000 mg/kg. Zn background limit is 6000 mg/kg, the threshold 11000 mg/kg and anomaly limit is 15000 mg/kg, respectively (Table 2).

4.3 Composite halo

The Zn/Pb and the Zn/(Pb+Zn) indices increase by moving away from the mineralization site, and this can be related to the mobility of Zn (Goodfellow et al., 1993). The fuzzy Zn/Pb index shows the Zn mineralization concentration in the northeast (Fig. 5 a). Zn/(Pb+Zn) is concentrated in northwest and the ratio of fuzzy Zn/(Pb+Zn) zonality index is low in the southwestern part of the area (Fig. 5 b)

4.4 Factor analysis

Factor analysis used in order to determine the relationship between variables and to reduce the dimensions of the data.

Table 1. Statistical parameters of Pb-Zn in Khomain area (mg/kg).

	Mean	Median	Minimum	Maximum	SD	Skewness	Kurtosis
Pb	5381	560	20	133930	16886	1.51	1.96
Zn	7268	1635	103	79180	13511	1.01	1.87

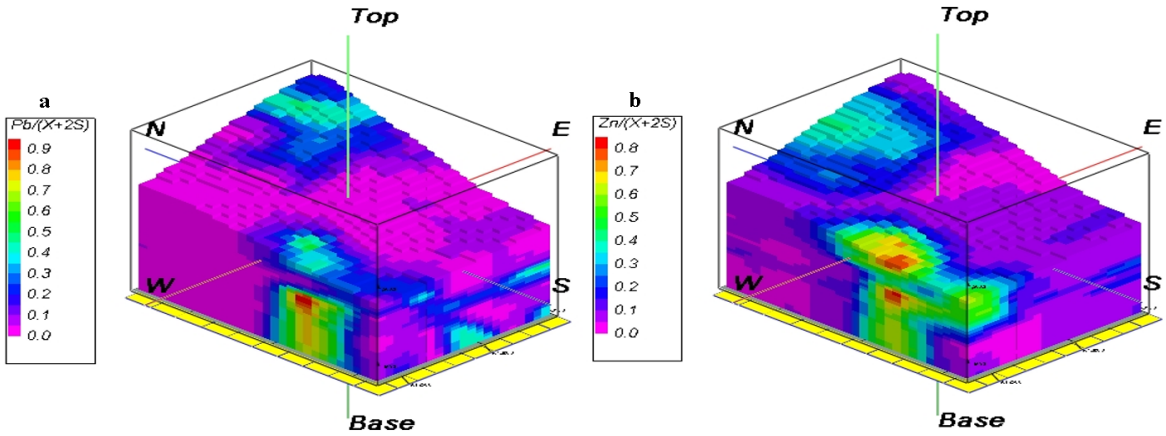

Figure 4. The values of (Median)+2S for fuzzy Pb and Zn.

Table 2. Pb and Zn background, threshold and anomaly range limit.

	Background	Threshold	Anomaly
Pb	4000-7000	7000-10000	10000-29000
Zn	6000-11000	11000-15000	15000-25000

Highest eigenvalue is related to the first component and is equal to 7.51, and the lowest value is related to the fifth component and is equal to 1.11 in factor analysis (Table 3). It can be seen that the number of 5 factors can justify approximately 71.34% of the total variability according to Table 3. The first factor has the most variance and justifies a large part of the variability alone among 5 selected factors. Therefore, variance is approximately 32.66% in the first factor. Variance is 21.05%, 6.76% and 4.83% in the second, third and fourth factor, respectively (Table 3). Pb with a load factor of 0.71 and Zn with a load factor of 0.73 participate in factors one and three, respectively (Table 3). The three-dimensional model of the first factor (Pb) ant third factor(Zn) shows that they have the highest anomaly with fuzzy number (GMP1) $0.7-0.9$ in the south-west of the study area (Fig. 6 a, b). Factor 1 indicates that probably chalcopyrite mineralization and Pb-Zn bearing and factor 2 alteration zones with clay formations. Factor 3 related to saline sediment and reduction effects and factor 5 may have basic rocks or weathering effects.

4.5 Singularity model

The slope of the fitted line is added to 3 to obtain α in the plotted graph (Li et al., 2021). Finally, the areas with α less than 3 represent enriched areas with positive singularity and the areas with α greater than 3 represent negative singularities. Areas with α equal to 3 are non-singular regions. The aim of the mineralized zone classification is to separate the different geochemical populations in the enriched areas. Therefore, $\alpha > 3$ representing the depleted areas were deleted. The singularity model is similar to the concentration-volume in fractal model, but, the concentration is replaced by α-singularity index and 3 the volume containing any α (Fig. 7 a).

The main enriched areas are divided into four Pb (Fig. 7 a) population levels and five Zn population level in the original singularity index (Fig. 7 b). The graph with the highest singularity index is introduced as areas with very weak mineralized zones. Therefore, the areas with very weak mineralized zones were removed from the rich areas (Ghadimi and Khavari, 2019).

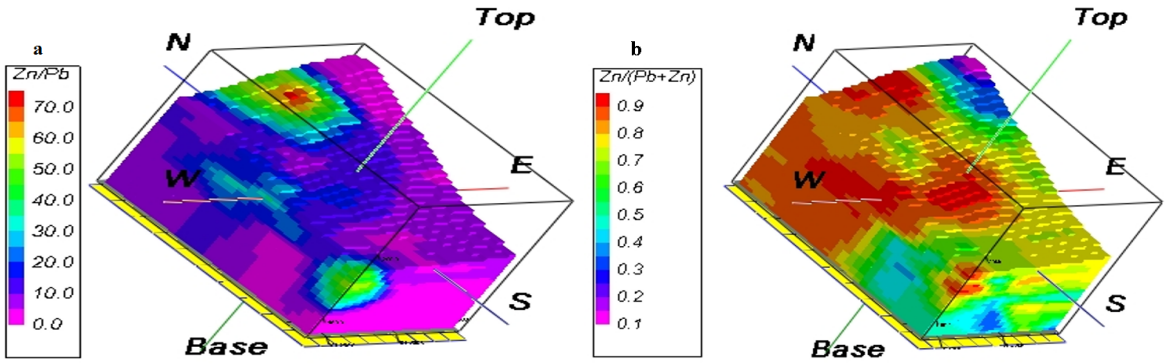

Figure 5. The fuzzy Zn/Pb and the fuzzy Zn/(Pb+Zn) indices in composite halo.

Table 3. Load factors of different metals with emphasis on Pb and Zn.

	Factor 1	Factor 2	Factor 3	Factor 4	Factor 5
Cr	-0.65	0.14	-0.10	0.63	0.02
Cu	0.26	0.06	0.47	-0.32	0.10
Fe	0.88	0.03	0.09	0.08	0.12
Mn	0.16	0.48	0.36	0.27	-0.23
Ni	-0.35	-0.01	-0.36	0.04	0.57
Pb	**0.71**	-0.05	0.46	0.09	0.06
Sr	0.10	-0.21	-0.01	-0.02	0.81
Ta	0.44	-0.14	0.63	-0.12	0.08
Zn	0.20	0.10	**0.73**	0.12	-0.15
Zr	-0.82	-0.01	-0.03	0.05	-0.24
Ti	-0.93	0.18	-0.13	0.02	0.16
Rb	-0.81	0.07	-0.20	0.12	0.26
V	-0.85	0.19	-0.16	0.05	0.30
Ba	-0.73	-0.14	-0.25	0.10	0.20
Na	-0.17	0.27	0.62	-0.07	-0.06
Mg	0.05	0.80	0.18	-0.05	-0.03
Al	-0.24	0.93	0.06	0.00	0.03
Si	-0.13	0.92	0.08	0.05	-0.03
P	-0.89	0.17	0.01	-0.05	-0.05
S	0.19	0.26	0.65	-0.04	-0.27
Cl	0.05	0.10	-0.03	0.90	0.01
K	-0.27	0.90	0.02	0.00	0.09
Ca	0.09	0.67	0.10	0.16	-0.24
Eigen value	7.51	4.84	1.55	1.39	1.11
Variance%	32.66	21.05	6.76	6.05	4.83
Cumulative variance%	32.66	53.70	60.46	66.51	71.34

The comparison of Pb and Zn mineralized zones is shown in the original singularity models in three-dimensional space in Fig. 8. The areas with a singularity index greater than 3 have been removed (background area) in Fig. 8. The mineralized zones are very poorly expressed and mineralization is located in southeast in Fig. 8 (a), (b) for Pb and Zn. The main enriched areas are divided into five Pb and Zn population levels in weighted singularity (Fig. 9 a, b).

The extent of strong mineralized zones in the weighted singularity is much greater than the original singularity (Fig. 10). The extent of weak to moderate mineralized zones is almost similar for Zn in the original singularity (Fig. 8 a,

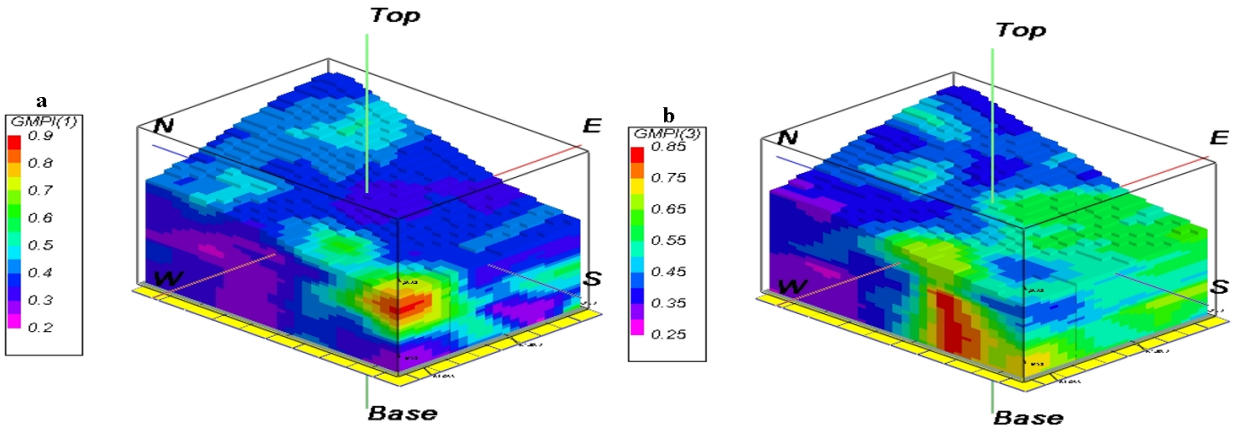

Figure 6. Pb and Zn distribution in fuzzy factor 1 and fuzzy factor 3.

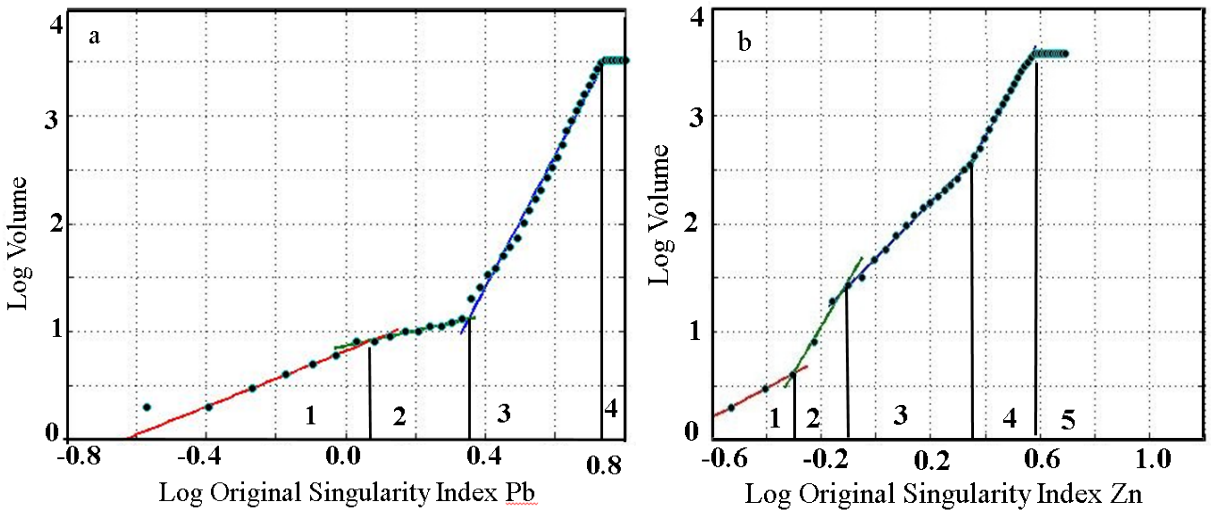

Figure 7. Original singularity index versus volume (a) Pb and (b) Zn.

b), but varies in strong mineralized zones (Fig. 10 a, b). However, the extent of weak to strong mineralized zones show a relatively similar for Pb and Zn in weighted singularity model (Fig. 10 a, b). On the other hand, the extent of each mineralized zones degree is much more in weighted singularity model than Pb and Zn in original singularity. In addition, mineralized zones trend is clear in the weighted singularity model. There is no clear mineralization trend in original singularity model.

Coefficient of areal association (CAA) is used to determine similarity of results of different methods. Taylor overlap coefficient (CAA) was used based on the Eq. (9) in this study.

$$\mathrm{CAA} = \frac{S_{AA} + S_{BB}}{S_{AB} + S_{BA} + S_{AA} + S_{BB}} \tag{9}$$

where S denotes area, indices are the geochemical populations, A is mineralized zone, and B shows background. In first and second models S_{AA} is area and S_{BA} is area in first model as background and in second model is mineralized zone (Shahrestani and Mokhtari, 2016). Coefficient of areal association were calculated for five models (Lepeltier, zonality, factor analysis, original singularity and weighted singularity model). Weighted singularity model is the best model in three dimension with more than 97% for Pb and more than 96% for Zn (Table 4). The mineralization has a northeast-southwest trend based on the weighted singularity and is matches with the trend of the normal faults in the mineralization place (Fig. 11).

5. Conclusion

The coefficient of areal association demonstrated that weighted singularity model was the sole indicator capable of detecting the boundary of Pb and Zn mineralization. Furthermore, the results indicated that mineralization processes have occurred from the north-east to the south-west parts of the study area. The weighted singularity model is suitable for the determination of geochemical anomalies in comparison to the lepeltier model, composite halo, factor analysis and original singularity models in three-dimensional space. Consequently, the integration of disparate models plays a pivotal role in the differentiation of anomalies from the background. The determination of weak anomalies, as well as the assessment of anomaly compliance with geological structures is the most important

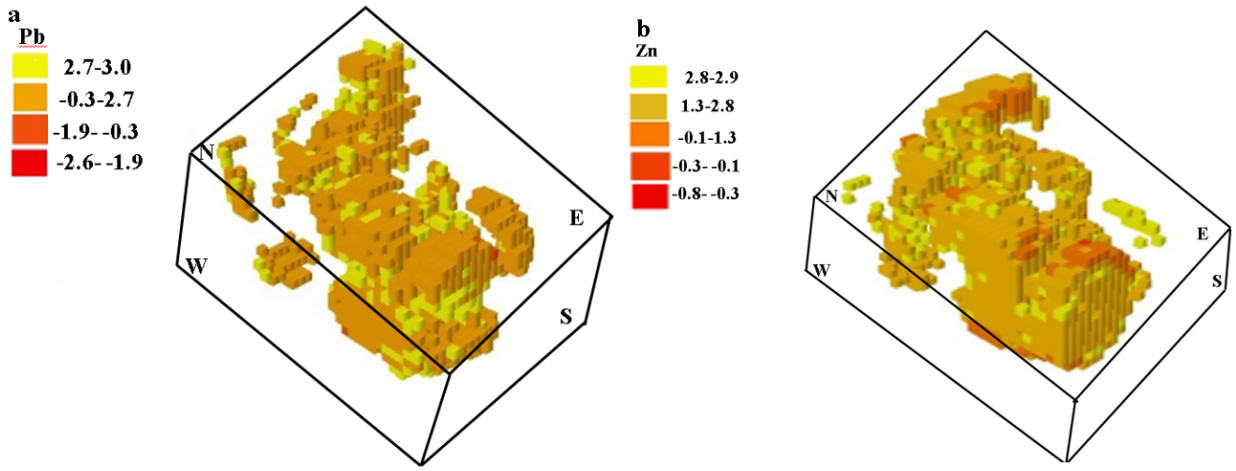

Figure 8. Distribution of original singularity index in three-dimensional mapping of Pb and Zn.

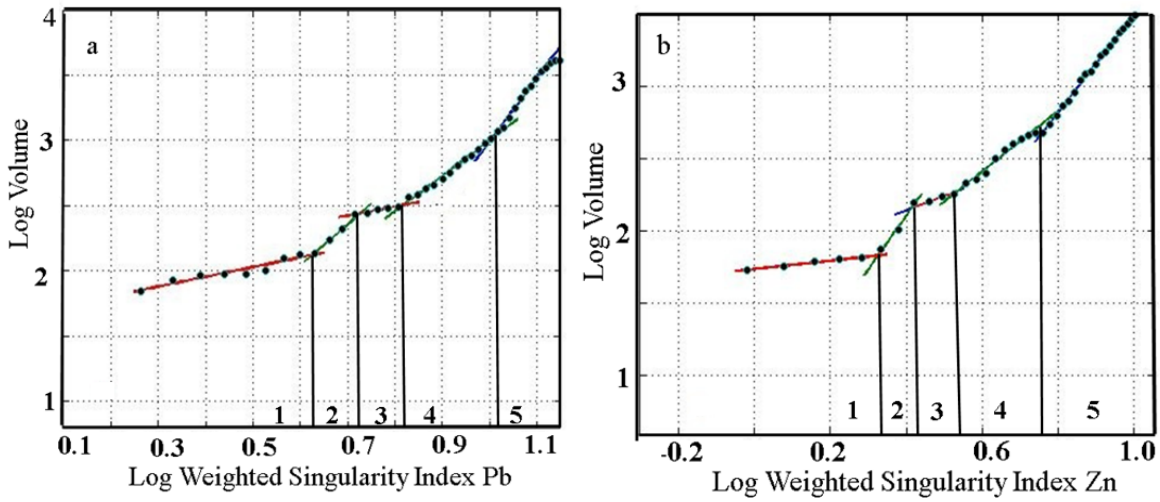

Figure 9. Weighted singularity index versus volume (a) Pb and (b) Zn.

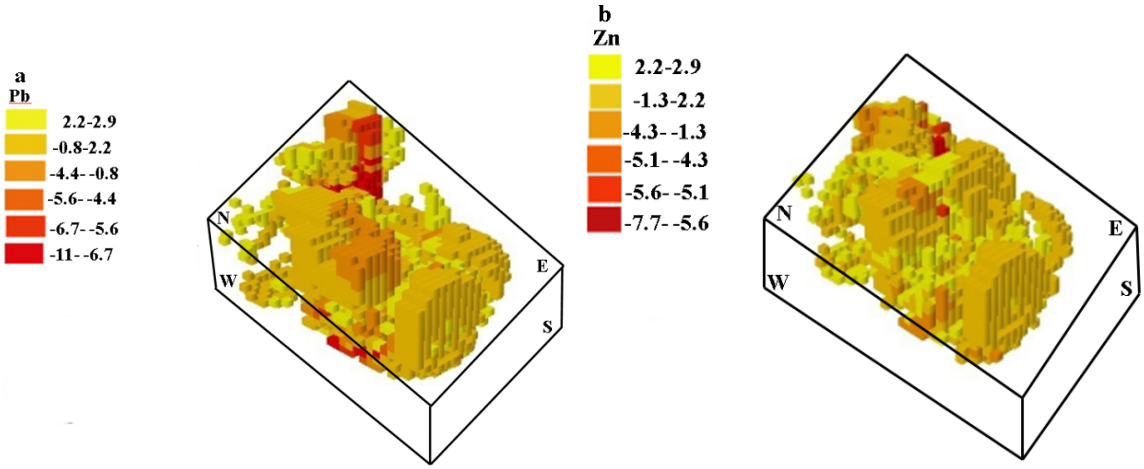

Figure 10. Distribution of weighted singularity index in three-dimensional mapping of Pb and Zn.

Table 4. Coefficient of areal association for different Pb and Zn models.

		L	Z	F	OS	WS
	L	1	-		-	-
Pb	Z	0.76	1		-	-
	F	0.84		1		-
	OS	0.82	0.85	0.89	1	-
	WS	0.96	0.92	0.91	0.97	1
	L	1	-		-	-
Zn	Z	0.40	1		-	-
	F	0.56	0.45	1	-	-
	OS	0.97	0.49	0.68	1	
	WS	0.86	0.91	0.92	0.96	1

L: Lepeltier; Z: Zonality; F: Factor analysis; OS: Singularity index; WS: Weighted singularity

It was found that anomaly trend in all the different methods of lepeltier, composite halo, factor analysis, original singularity and weighted singularity are northeast and southwest according to the three-dimensional shapes. But the severity of anomalies is different in them. For example, anomaly extent is very high in the zonal halo model (Fig. 5). Anomalous extent can also be seen in the weighted singularity model, but the separation of lower and higher anomaly is clear in the weighted singularity model due to the accuracy of the border method.

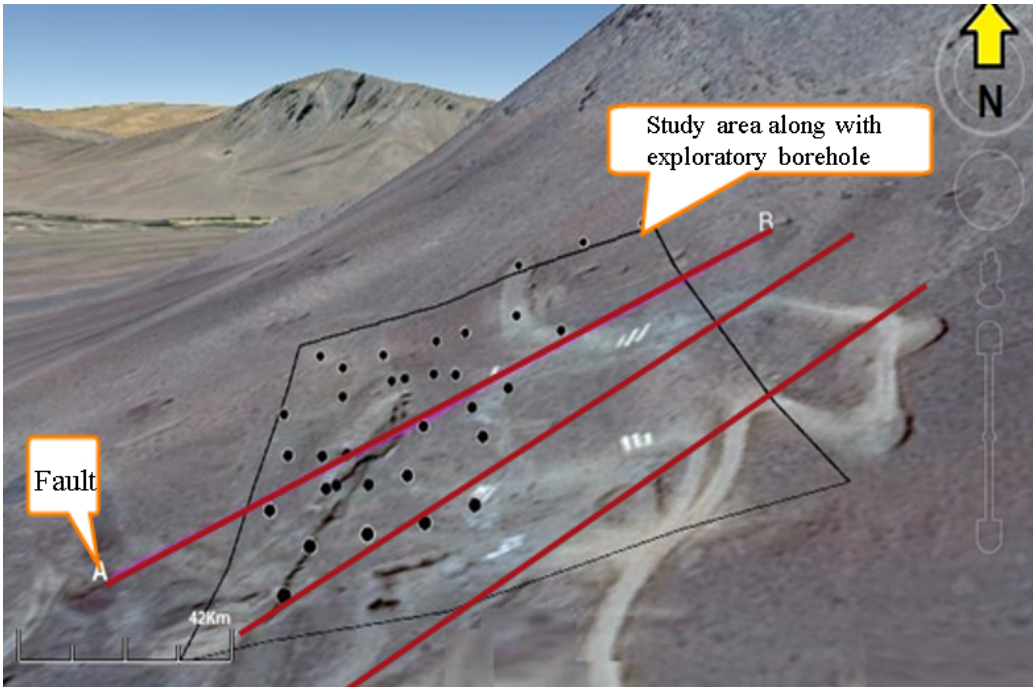

Figure 11. Exploration area of Pb and Zn in Khomain.

in the delineation of the extent and expansion of Pb and Zn in Khomain area, and is important in the identification of the general Pb and Zn northeast-southwest trend of mineralization.

Authors contributions
The First author, Fridon Ghadimi, has prepared the manuscript and done the research. The second author, Massume has prepared the figures.

Availability of data and materials
The data that support the findings of this study are available from the corresponding author, upon reasonable request.

Conflict of interests
The authors declare that they have no known competing financial interests or personal relationships that could have appeared to influence the work reported in this paper.

References

Afzal P., Heidari S. M., Ghaderi M., Yasrebi A. B. (2017) Determination of mineralization stages using correlation between geochemical fractal modeling and geological data in Arabshah sedimentary rock-hosted epithermal gold deposit, NW Iran. *Ore Geology Review* 91:278–295. DOI: https://doi.org/10.1016/j.oregeorev.2017.09.021.

Ali K., Cheng Q., Chen Z. (2015) Multifractal power spectrum and singularity analysis for modeling stream sediment geochemical distribution patterns to identify anomalies related to gold mineralization in Yunnan Province, South China. *Geochemical Exploration Environment Analysis* 7 (4): 293–301. DOI: https://doi.org/10.1144/1467-7873/06-1.

Alipoor R., Hajiloo S. Z., Hosseinkhani A. (2021) Structural analysis of the Takiyeh Zn-Pb mine in the Malayer-Esfahan metallogenic belt, west Iran. *Journal of Economic Geology* 13 (3): 627–643. DOI: https://doi.org/10.22067/ECONG.V13I3.86454.

Arjmandzadeh R., Rashvanlou V. S., Dabiri R., Almasi A. (2017) Satellite thermal surveys to detecting hidden active faults and fault termination, Case study of Quchan fault, NE Iran. *Iranian Journal of Earth Sciences* 9 (1): 39–47.

Behera S., Naliy Panigrah M. K. (2021) Mineral prospectivity modelling using singularity mapping and multifractal analysis of stream sediment geochemical data from the auriferous Hutti-Maski schist belt, S. India. *Ore Geology Reviews* 131:104029. DOI: https://doi.org/10.1016/j.oregeorev.2021.104029.

Bigdeli A., Maghsoudi R., Ghezelbash R. (2023) Recognizing Geochemical Anomalies Associated with Mineral Resources Using Singularity Analysis and Random Forest Models in the Torud-Chahshirin Belt, Northeast Iran. *Minerals* 13 (11) DOI: https://doi.org/10.3390/min13111399.

Chen X., Xu R., Zheng Y., Jiang X., Du W. (2018) Identifying potential Au-Pb-Ag mineralization in SE Shuang koushan, North Qaidam, West China: Combined log-ratio approach and singularity mapping. *Journal of Geochemical Exploration* 189:109–121. DOI: https://doi.org/10.1016/j.oregeorev.2021.104029.

Cheng Q. (2007) Mapping singularities with stream sediment geochemical data for prediction of undiscovered mineral deposits in Gejiu, Yunnan Province, China. *Ore Geology Reviews* 32:314–324. DOI: https://doi.org/10.1016/j.oregeorev.2006.10.002.

——— (2008) Non-linear Theory and Power-Law Models for Information Integration and Mineral Resources Quantitative Assessments. *Progress in Geomathematics,* 195–225. DOI: https://doi.org/10.1007/s11004-008-9172-6.

Cheng Q., Bonham-Carter G. F., Wang W., Zhang S., Li W., Xia Q. (2011) A spatially weighted principal component analysis for multi-element geochemical data for mapping locations of felsic intrusions in the Gejiu mineral district of Yunnan, China. *Computer & Geoscience* 37 DOI: https://doi.org/10.1016/j.cageo.2010.11.001.

Elmi R., Arian M. A., Ashja Ardalan A., Yazdi A. (2025) Petrology of volcanism in the Alasht-Haraz road of the Alborz mountain range, south of Amol (north of Iran). *Iranian Journal of Earth Sciences* 17 (3) DOI: https://doi.org/10.57647/j.ijes.2025.16800.

Fan W., Liu G., Chen O., Lu L., Cui Z., Zuo B., Wu X. (2024) Extraction of weak geochemical anomalies based on multiple-point statistics and local singularity analysis. *Computer and Geoscience* 28:157–173. DOI: https://doi.org/10.1007/s10596-024-10272-3.

Ghadimi F., Khavari M. (2019) Comparison of original and weighted singularity index in separation of Pb- Zn mineralized zone in the Haft Savaran district, central Iran *Iranian Journal of Earth Sciences* 11:1–16. DOI: https://doi.org/10.30495/IJES.2019.665321.

Gonçalves M. A., Pinto F., Vieira R. (2018) Using multifractal modelling, singularity mapping, and geochemical indexes for targeting buried mineralization: Application to the W-Sn Panasqueira ore-system, Portuga. *Journal of Geochemical Exploration* 189:42–53. DOI: https://doi.org/10.1016/j.gexplo.2017.07.008.

Goodfellow W. D., Lydin J. W., Turner R. (1993) Geology and genesis of stratiform sediment-hosted (sedex) zinc-lead-silver sulfide deposits. In: Mineral Deposit Modeling. *Geological Association of Canada, Special Paper* 40:201–251. DOI: https://doi.org/10.1016/B978-0-08-095975-7.01109-8.

Hu X., Li H., Förster M. W., Elatikpo S. M., Kong H., Wu J., Zhu D. (2023) Using apatite to differentiate metallogenic potential and environment of granitic rocks: A case study from the Tongshanling W-Sn-Cu-Pb-Zn ore field, Nanling Range (South China). *Journal of Geochemical Exploration* 245:107143. DOI: https://doi.org/10.1016/j.gexplo.2022.107143.

Huang C., Du G., Jiang H. O., Xie J., Zha D., Li H., Lai C. K. (2019a) Ore-forming fluids characteristics and metallogenesis of the Anjing Hitam Pb-Zn Deposit in Northern Sumatra, Indonesia. *Journal of Earth Science* 30 (1): 131–141. DOI: https://doi.org/10.1007/s12583-019-0859-z.

Huang C. W., Li H., Lai C. K. (2019b) Genesis of the Binh Do Pb-Zn deposit in northern Vietnam: Evidence from H-O-S-Pb isotope geochemistry. *Journal of Earth Science* 30 (4): 679–688. DOI: https://doi.org/10.1007/s12583-019-0872-2.

Karami K., Afzal P. (2015) Application of multifractal modeling for separation of sulfidic mineralized zones based on induced polarization and resistivity data in the Ghare-Tappeh Cu deposit, NW Iran. *Iranian Journal of Earth Sciences* 2 (7): 134–141. https://doi.org/sanad.iau.ir/en/Article/9

Li C., Liu B., Guo K., Li B., Kong Y. (2021) Regional Geochemical Anomaly Identification Based on Multiple-Point Geostatistical Simulation and Local Singularity Analysis-A Case Study in Mila Mountain Region, Southern Tibet. *Minerals* 11 (10): 1037. DOI: https://doi.org/10.3390/min11101037.

Liu Y., Carranza E. J. M. (2022) Uncertainty Analysis of Geochemical Anomaly by Combining Sequential Indicator Co-simulation and Local Singularity Analysis. *Natural Resources Research* 31:1889–1908. DOI: https://doi.org/10.1007/s11053-021-10001-y.

Liu Y., Cheng Q., Carranza E. J. M., Zhou K. (2019) Assessment of geochemical anomaly uncertainty through geostatistical simulation and singularity analysis. *Natural Resources Research* 28:199–212. DOI: https://doi.org/10.1007/s11053-018-9388-1.

Luo D., Zeng G. (2018) Application and effects of singularity analysis in evaluating the denudation degree of Carlin-type gold deposits in southwest Guizhou, China. *Ore Geology Review* 96:164–180. DOI: https://doi.org/10.1016/j.oregeorev.2018.04.018.

Nazari Sarem M., Dabiri R., Ansari M. R., Vosoughi Abedini M. (2020) Estimate of shore geomorphology fractal dimension north of Persian Gulf by box–counting method. *Quantitative Geomorphological Research* 9 (2): 159–174.

Parsa M., Maghsoudi A., Carranza E. J. M., Yousefi M. (2017a) Enhancement and mapping of weak multivariate stream sediment geochemical anomalies in Ahar Area, NW Iran. *Natural Resources Research* 26 (4): 443–455. DOI: https://doi.org/10.1007/s11053-017-9346-3.

Parsa M., Maghsoudi A., Yousefi M., Sadeghi M. (2017b) Multifractal analysis of stream sediment geochemical data: Implications for hydrothermal nickel prospection in an arid terrain, eastern Iran. *Journal of Geochemical Exploration* 181:305–317. DOI: https://doi.org/10.1016/j.gexplo.2016.11.013.

Reimann C., Filzmoser P., Garrett R. G. (2005) Background and threshold: critical comparison of methods of determination. *Sciences. Total Environment* 346:1–16. DOI: https://doi.org/10.1016/j.scitotenv.2004.11.023.

Saadat S., Ghoorchi M., Dabiri R. (2023) Extracting clay minerals with emphasis on Bentonite in Eastern Iran, using Landsat 8 and ASTER images. *Iranian Journal of Earth Sciences* 15 (3): 188–194. DOI: https://doi.org/10.30495/ijes.2023.1973739.1815.

Sadeghi B. (2021) Concentration-concentration fractal modelling: A novel insight for correlation between variables in response to changes in the underlying controlling geological-geochemical processes. *Ore Geology Review* 128:103875. DOI: https://doi.org/10.1016/j.oregeorev.2020.103875.

Salehpour S., Arian M. A., Rad Zarei Sahamieh R. A. J., Yazdi A. (2025) Geochemistry and technomagmatic environment of Eocene volcanic rocks in Yuzbashi Chay region, west of Qazvin (Iran). *Iranian Journal of Earth Sciences* 17 (1): 1–13. DOI: https://doi.org/10.57647/j.ijes.2025.1701.04.

Shahrestani Sh., Mokhtari A. R. (2016) Dilution correction equation revisited: The impact of stream slope, relief ratio and area size of basin on geochemical anomalies. *African Earth Sciences* 128:16–26. DOI: https://doi.org/10.1016/j.jafrearsci.2016.06.019.

Stocklin J., Nabavi M. (1972) Tectonic Map of Iran, scale: 1:100,000. *Geological Survey of Iran*

Taylor R. D., Leach D. L., Bradley D. C., Pisarevsky S. A. (2009) Compilation of Mineral Resource Data for Mississippi Valley-Type and Clastic-Dominated Sediment-Hosted Lead-Zinc Deposits. U. S. Geological Survey Open-File Rep–1297. 42 DOI: https://doi.org/10.3133/ofr20091297.

Vincent V. I., Li H., Girei M. B., Ahmed H. A., Ntekim E. E. (2021) Genesis and age of Pb-Zn mineralization from the Ningi-Burra ring complex, North Central Nigeria: Constraints from zircon morphology, U-Pb dating and Lu-Hf isotopes. *Lithos,* 106115. DOI: https://doi.org/10.1016/j.lithos.2021.106115.

Wang J., Zuo R. (2019) Recognizing geochemical anomalies via stochastic simulation-based local singularity analysis. *Journal of Geochemical Exploration* 198:29–40. DOI: https://doi.org/10.1016/j.gexplo.2018.12.012.

Xiao F., Chen J., Hou W., Wang Z., Zhou Y., Erten O. (2018) A spatially weighted singularity mapping method applied to identify epithermal Ag and Pb-Zn polymetallic mineralization associated geochemical anomaly in Northwest Zhejiang, China. *Journal of Geochemical Exploration*

Yazdi A., Ashja-Ardalan A., Emami M. H., Dabiri R., Foudazi M. (2019) Magmatic interactions as recorded in plagioclase phenocrysts of quaternary volcanics in SE Bam (SE Iran). *Iranian Journal of Earth Sciences* 11 (3): 215–224. DOI: https://doi.org/10.30495/ijes.2019.667379.

Yousefi M., Kamkar-Rouhani A., Carranza E. J. M. (2012) Geo-chemical mineralization probability index (GMPI): A new approach to generate enhanced stream sediment geochemical evidential map for increasing probability of success in mineral potential mapping. *Journal of Geochemical Exploration* 115:24–35. DOI: https://doi.org/10.1016/j.gexplo.2012.02.002.

Yu H., Tang J., Li H., Kang H. (2020) Metallogenesis of the Siding Pb-Zn deposit in Guangxi, South China: Rb-Sr dating and C-O-S-Pb isotopic constraints. *Ore Geology Reviews* 121:103499. DOI: https://doi.org/10.1016/j.oregeorev.2020.103499.

Zandy Ilghani N., Ghadimi F., Ghomi M. (2018) Application of alteration index and zoning for Pb-Zn exploration in Haft-Savaran area, Khomein, Iran. *Journal of Mining & Environment* 9:229–242. DOI: https://doi.org/10.22044/jme.2017.6128.1427.

Zhang D. J., Cheng Q. M., Agterberg F. P., Cheng Z. J. (2016) An improved solution of local window parameters setting for local singularity analysis based on Excel VBA batch processing technology. *Computer Geoscience* 88:54–66. DOI: https://doi.org/10.1016/j.cageo.2015.12.012.

Zhang Z. B., Zhu Z. J., Li H., Jiang W. C., Wang W. F., Xu Y., Li L. R. (2020) Provenance and salt structures of gypsum formations in the Pb-Zn ore-bearing Lanping basin, Southwest China. *Journal of Central South University* 27:1828–1845. DOI: https://doi.org/10.1007/s11771-020-4411-1.

Zhao J., Chen S., Zuo R. (2017) Identification and mapping of lithogeochemical signatures using staged factor analysis and fractal/multifractal models. *Geochemical Exploration Environment Analysis* 17 (3): 239–251. DOI: https://doi.org/10.1144/geochem2016-013.

——— (2015) Identifying geochemical anomalies associated with Au–Cu mineralization using multifractal and artificial neural network models in the Ningqiang district, Shaanxi, China. *Journal of Geochemical Exploration* 164:33–41. DOI: https://doi.org/10.1016/j.gexplo.2015.06.018.

Zhao J., Wang W. L., Cheng Q. M., Agterberg F. P. (2016) Mapping of Fe mineral potential by spatially weighted principal component analysis in the eastern Tianshan mineral district, China. *Journal of Geochemical Exploration* 164:107–121. DOI: https://doi.org/10.1016/j.gexplo.2015.11.004.

Zhou Y., Zhang Z., Yang J., Ge Y., Cheng Q. (2022) Machine Learning and singularity analysis reveal zircon fertility and magmatic intensity: implications for porphyry copper potential. *Natural Resources Research* 31:3061–3078. DOI: https://doi.org/10.1007/s11053-022-10122-y.

Zhu D., Li H., Jiang W., Wang C., Hu X., Kong H. (2022a) Ore-forming environment of Pb-Zn mineralization related to granite porphyry at Huangshaping skarn deposit, Nanling Range, South China. *Transactions of Nonferrous Metals Society of China* 32:3015–3035. DOI: https://doi.org/10.1016/S1003-6326(22)66000-X.

Zhu D. P., Li H., Tamehe L. S., Jiang W. C., Wang C., Wu K. Y. (2022b) Two-stage Cu-Pb-Zn mineralization of the Baoshan deposit in southern Hunan, South China: Constraints from zircon and pyrite geochronology and geochemistry. *Journal of Geochemical Exploration* 24:107070. DOI: https://doi.org/10.1016/j.gexplo.2022.107070.